

RESPONSE TO REVIEWERS

Reviewer 1

Comment 1

it [the ms.] still suffer some important points that needs to be addressed. 1) The first one is that the overall interpretation seems heavily model driven. Indeed the E-W fractures are interpreted as forebulge-parallel extension, which make sense, but the systematic attribution of the N-S fractures to across strike extension can be argued against: - an alternate interpretation would be to consider the N-S fractures as related to LPS, postponing the E-W, forebulge related fractures, leading to similar patterns than the one described.

Response: Done.

We thank the reviewer for this comment. We have added this text:

“LPS is to be excluded, as the state of stress in this case would include a positive minimum stress (Fig. 1). In agreement, LPS-related extensional structures can form only due to fluid pressure contribution and they include mm- to cm-long fractures filled with calcite (which is removed from pressure solution seams, Fig. 1; Tavani et al., 2015 and references therein). The type (joints with no calcite infill) and size (tens of m-long) of transverse extensional structures described here are incompatible with the layer-parallel shortening mechanism.

Comment 2

The occurrence of a NNESSW (what is the mean strike of it?) goes well into this alternate scenario, as the Ebro Basin underwent a regional 20° Clockwise rotation during Paleogene, as reconstructed by the paleomagnetic data (Parés et al., 1988, Physics of the Earth and Planetary Interiors, Volume 52, Issue 3-4, p. 267-282). This rotation does not seem to have been considered by the authors, and I think this needs addressed.

Response: Not agreed.

It has been recently demonstrated (after the initial papers describing paleomagnetic data in the Triassic red beds) that the Ebro basin has not experienced a general rotation during the Paleogene. Paleogene vertical-axis rotations in the Pyrenees are mainly related with displacement gradients of the thrust sheets, mostly resulting from the distribution of the Triassic salt detachment horizon (Sussman et al., 20014; Soto et al., 2006; Muñoz et al., 2013). In addition, older vertical axis rotations, can be related with the extensional and sinistral displacement of Iberia during Early Cretaceous (Dinarès-Turell and García-Senz, 2000; Gong et al., 2009).

Apart from these vertical axis rotations, which are at present well documented, the Ebro basin and in detailed the eastern part of the Ebro basin where this study has been located has not experienced any vertical-axis rotation as documented by paleomagnetic studies (Burbank et al., 1992; Taberner et al., 1999).

Burbank, D. W., Puigdefàbregas, C., & Muñoz, J. A. (1992). The chronology of the Eocene tectonic and stratigraphic development of the eastern Pyrenean foreland basin, northeast Spain. *Geological Society of America Bulletin*, 104(9), 1101–1120. [http://doi.org/10.1130/0016-7606\(1992\)104<1101:TCOTET>2.3.CO;2](http://doi.org/10.1130/0016-7606(1992)104<1101:TCOTET>2.3.CO;2)

Dinarès-Turell, J., & Senz, J. G. (2000). Remagnetization of Lower Cretaceous limestones from the southern Pyrenees and relation to the Iberian plate geodynamic evolution. *Journal of Geophysical Research: Solid Earth* (1978–2012), 105(B8), 19405–19418. <http://doi.org/10.1029/2000JB900136>

Gong, Z., van Hinsbergen, D. J. J., Vissers, R. L. M., & Dekkers, M. J. (2009). Early Cretaceous syn-rotational extension in the Organyà basin—New constraints on the palinspastic position of Iberia during its rotation. *Tectonophysics*, 473(3-4), 312–323. <http://doi.org/10.1016/j.tecto.2009.03.003>

Soto, R., Casas-Sainz, A. M., & Pueyo, E. L. (2006). Along-strike variation of orogenic wedges associated with vertical axis rotations. Journal of Geophysical Research: Solid Earth, 111(B10), B10402. <http://doi.org/10.1029/2005JB004201>

Sussman, A. J., Butler, R. F., Dinarès-Turell, J., & Vergés, J. (2004). Vertical-axis rotation of a foreland fold and implications for orogenic curvature: an example from the Southern Pyrenees, Spain. Earth and Planetary Science Letters, 218(3-4), 435–449. [http://doi.org/10.1016/S0012-821X\(03\)00644-7](http://doi.org/10.1016/S0012-821X(03)00644-7)

Taberner, C., Dinarès-Turell, J., Giménez, J., & Docherty, C. (1999). Basin infill architecture and evolution from magnetostratigraphic cross-basin correlations in the southeastern Pyrenean foreland basin. Geological Society of America Bulletin, 111(8), 1155.

Comment 3

Two important things are missing to back up the interpretation of the authors: relative chronology; and observation and report of systematic occurrence of N-S joints with E-W joints.

Response: Done

The few E-W striking joints systematically abut on the N-S striking set, indicating that E-W striking joints are cross-joints formed perpendicular to the master (N-S) joint set. This is well shown in figures 2D and 2E (for the NNW-SSE striking set), and it is now mentioned in the revised text.

Comment 4

I would be interested to see reported the length of the fracture tracks for each set, I am sure it could be of interest as well to solve the problem I mentioned in my first comment.

Response: Done

Graph added in figure 3f

There is also minor remarks:

Comment 5

Page 2, line 26-27: "Even in arched systems, the forebulge, the foredeep, and the belt tend to be nearly parallel to each other locally" → can you report related references?

Response: Done

Added

Comment 6

Page 4, line 28-29: "The NE and SE portions of the study area are highly vegetated (Fig. 3d,e) and only a few joint traces have been mapped there." → how does it affect the statistic? Why not leaving these out?

Response: Done

We agree. Nodes with < 20 data have not been considered in our analysis. This is now mentioned in the text.

Comment 7

Page 5: Why did you choose these lengths for the triangular mesh? Do you need it to be one order of magnitude longer than the longest fractures? Can you discuss the impact?

Response: Done

The radius of the circular moving window is set to these values for these two reasons: 1) it is two orders of magnitude longer than the average length of joints; 2) it is larger enough to ensure that at each node the data number is >20. This is now explicated in the text

Comment 8

Figure 2 C-F: The north is not really clear from this representation.

Response: Done

North added.

Reviewer 2

Comment 1

In the introduction, you outline a mechanism to explain transverse jointing in the foreland. Then you continue with the outlook that the acquired remote sensing data allows to investigate the primary mechanism for this joint formation. Hence I wonder: Haven't you proposed already before the data collection and discussion of what the primary mechanism is? Does this lead to a bias in the data interpretation? Maybe it would be better to present the model after the data presentation in the discussion to avoid that such an impression might arise.

Response: Not agreed.

This is a matter of writing style and not a source of bias. In our view the rationale of the work and the state of the art must include a brief introduction to the causative geological processes allowing to understand data.

Comment 2

Also on that regard, a discussion on the potential driving force behind the suggested orogen-parallel stretching of the foreland basin is largely missing (or well hidden, in case I missed it), which would be very interesting though.

Response: Done

We have added this text in the discussion: *The basic concept behind this mechanism is the following: when a straight line joining two fixed points - the tips of a fault in the case of Destro (1995) or the edges of the foredeep in the case of Quintà and Tavani (2012) – becomes an arch, there is stretching (Fig. 1b), which causes extensional stress parallel to the direction of elongation. In essence, this mechanism is expected to operate in any doubly plunging foredeep, particularly at its lateral edges, such as in the study area (Fig. 3a)*

Comment 3

In the introduction, it is briefly referred to two publications invoking the possibility of lithospheric bending to account for such kind of stretching (Doglioni, 1995; Quintà and Tavani, 2012; although the process described by Doglioni is regarded as not applicable for the study area, which is comprehensible). In the discussion, this subject is covered with only two sentences (page 7 line 31 to page 8 line 3; half of it being a repetition of the introduction statement). Here, foreland-parallel stretching is suggested to form the N-S joints and an analogue reference is made to the process of release faulting (Destro, 1995). I think this requires much more attention: Destro (1995) describes a purely extensional setting and it is therefore not straightforward to understand how this applies to the Pyrenean foreland, especially in the light that you propose foreland-parallel extension from the Paleocene until the end of convergence (page 7, line 22). Hence, I believe a more elaborate discussion for the use of this model is necessary, in particular, and potential driving mechanism for such stretching, in general.

Response: Done

See response to the previous point.

Comment 4

Adding to this, you mention the westward plunge of the foredeep basin and refer to figure 3a. I am not sure if this is it actually visible in the figure or if it requires previous knowledge of the region to identify it!? I think an E-W cross-section would be very helpful.

Response: Done

We have added the trace of the axis of the foredeep basin in figure 3 to show its W-ward plunge.

Comment 5

A second issue revolves around the timing of joint formation. You state that the dominant N-S trending joint system formed prior to folding and refer to figure 2b, where joints are supposedly tilted. Unfortunately, from the picture alone, it is very hard to see this. How did you determine that these joints are tilted? How can you exclude the possibility of joint formation after folding? Such a determination appears to me as a very difficult asset, since you would have to know their original orientation and at the same time line out why its present orientation is not the original one. I think this is a very important issue that needs to be clarified.

Response: Done

Timing of deformation is rather evident from figure 2. We have improved the description of this figure: *In the field, joints are constantly bedding-perpendicular, regardless of the bedding dip (Fig. 2a,b), and they are characterized by the occurrence of either a single set (Fig. 2c) or by a ladder pattern (Fig. 2d,e). In the latter case, the few E-W striking joints are almost everywhere perpendicular to the N-S striking set and abut on it (Fig. 2e). This indicates that E-W striking joints are cross-joints formed perpendicular to, and about synchronously with, the N-S striking joint set*

Comment 6

A second argument for the age of joints is their absence in Quaternary sediments. First, there is still a large age span from the Quaternary to the Eocene (using the word “evidence” (page 7, line 9) for an Eocene formation age is therefore maybe a stretch), and second: what is the character of these sediments? Are they solidified to a degree where fractures would be able to form in case the joints in the Eocene rock were of Quaternary age?

Response: Done

See response to previous point.

Comment 7

Another thing: As you have been in the field, it would be great to see a comparison of field data with the remote lineament data. E.g. do the joints have a preferential dip direction, are they all just vertical?

Response: Done

We have added stereoplots of joints collected in the northern portion of the study area.

Comment 8

Figure 1: This is a very nice figure, but some features can only be identified when zooming in a lot, i.e. the text “peripheral bulge”, veins, and stylolites. Please improve this. Also, I recommend to place the names forebulge, foredeep, foreland fold-andthrust belt into/above the block figure and not just mention them in the figure caption.

Response: Done

Labels added.

Comment 9

Figure 2:

- 1) please show the locations of these outcrops in figure 3.
- 2) Also, I would prefer to show field photos after showing a map of the study area.
- 3) In Figure 2b, please point at the joints as it is not super clear that the big surface is, I assume, the bedding surface.

Response: Partly agreed

- 1) This cannot be done due to the size of the figure: the labels of the five sites would cover much of the figure.
- 2) In the text the figure 2 is called before figure 3, so it cannot be shown before.

3) Yes, the south-dipping surface is the bedding, this is now mentioned.

Comment 10

Figure 3: add some placemarks (e.g. towns) to the map, so that it's a bit easier for the reader to capture the location of the study area. (took me a little bit to find the exact area on google earth).

Response. Done.

Added

Comment 11

Figure 5: I think it would be really nice, if you exemplarily show a few rose plots (joint length-weighted) for different colored regions in figure 5. I believe this would make it much easier for the reader to understand how to read the color code of the figure.

Response: Done

This is probably a misunderstanding. The colour code refers to the dispersion of azimuthal data, which is not well appreciable in rose diagrams as the dominant set is much developed than the other sets. We have improved the caption of the figure.

1 **Transverse jointing in foreland fold-and-thrust belts: a remote sensing
2 analysis in the eastern Pyrenees**

3

4 | Stefano Tavani¹, Pablo Granado², Amerigo Corradetti³, Thomas Seers³, [Josep Maria Casas²](#),
5 | Josep Anton Muñoz²

6

7 | 1 - DISTAR, Università degli Studi di Napoli “Federico II”, Via Cupa Nuova Cintia 21,
8 | 80126, Naples, Italy

9 | 2 - Institut de Recerca Geomodels, Departament de Dinàmica de la Terra i de l’Oceà,
10 | Universitat de Barcelona, C/ Martí i Franques s/n, 08028, Barcelona, Spain

11 | 3 - Department of Petroleum Engineering, Texas A&M University at Qatar. Education City,
12 | PO Box 23874, Doha, Qatar

13

14 **Abstract**

15 | Joint systems in the eastern portion of the Ebro Basin of the eastern Pyrenees enjoy near
16 | continuous exposure from the frontal portion of the belt up to the external portion of its
17 | associated foredeep. Utilizing orthophoto mosaics of these world class exposures, we have
18 | manually digitized over 30000 joints within a 16x50 km study area. The mapped traces
19 | exhibit orientations that are dominantly perpendicular to the trend of the belt (transverse) and,
20 | subordinately, [orthogonalparallel](#) to [#the_belt](#) (longitudinal). In particular, joints
21 | systematically orient perpendicular to the trend of the belt both in the frontal folds and in the
22 | inner and central portion of the foredeep basin. Longitudinal joints occur rarely, with a
23 | disordered spatial distribution, exhibiting null difference in abundance between the belt and
24 | the foredeep. Joint orientations in the external portion of the foredeep become less clustered,
25 | with adjacent areas dominated by either transverse or oblique joints. Our data indicates that
26 | joints in the studied area formed in the foredeep in response to a foredeep-parallel stretching,
27 | which becomes progressively less intense within the external portion of the foredeep. There,
28 | the minimum stress direction becomes more variable, evidencing poor contribution of the
29 | forebulge-perpendicular stretching on stress organization.

30

1 **Introduction**

2 Fractures can be effective pathways for fluid flow (e.g. Laubach et al., 2019), thus
3 impacting production of hydrocarbons (Barr et al., 2007; Engelder et al., 2009; Questiaux et
4 al., 2010) and geothermal water (Haffen et al., 2013; Vidal et al., 2017), the pathways and
5 fates of contaminants released from deep geological radioactive waste repositories
6 (Berkowitz et al., 1988; Iding and Ringrose, 2010) and the sustainable management of
7 groundwater (Masciopinto and Palmiotta, 2013). Associated with crustal tension, joints are
8 ubiquitous open-mode fractures occurring in a range of tectonic settings, including collisional
9 belts. In collisional settings, layer bending and stretching during the growth of thrust-related
10 anticlines has conventionally been invoked as the principal causative process for the
11 development of joints oriented approximately parallel (e.g. Ramsay, 1967; Murray, 1968) and
12 perpendicular (e.g. Dietrich, 1989; Lemiszki et al., 1994) to the trend of the belt and of the
13 thrust related anticlines. However, the frequently observed obliquity between joints (and
14 other meso-scale structures) and the trend of the hosting anticlines (e.g. Tavani et al., 2019;
15 Beaudoin et al., 2020), along with the documented occurrence of joints in exposed forelands
16 (e.g. Dunne and North, 1990; Zhao and Jacobi, 1997; Billi and Salvini, 2003; Whitaker and
17 Engelder, 2006), has more recently led to the conclusion that, in many cases, joints and other
18 kinds of extensional fractures exposed in thrust and fold belts have developed prior to folding
19 and thrusting, within the foreland region (e.g. Doglioni, 1995; Zhao and Jacobi, 1997;
20 Tavarnelli and Peacock, 1999; Lash and Engelder, 2007; Branellec et al., 2015; Basa et al.,
21 2019; Giuffrida et al., 2019; Martinelli et al., 2019; Carrillo et al., 2020), where joints are
22 layer-perpendicular and commonly oriented parallel (longitudinal) and perpendicular
23 (transverse) to the belt-foredeep-forebulge trend (Tavani et al., 2015).

24 A partially unresolved question in foreland deformation relates to the development of
25 transverse joints, which requires a tensile minimum stress oriented parallel to the foredeep.
26 Even in arched systems, the forebulge, the foredeep, and the belt tend to be nearly parallel to
27 each other locally ([e.g. the Hellenic arc, the Apennines-Calabrian arc, the Betic-Rif arc](#)). The
28 shortening direction in the inner portion of the foredeep (subjected to layer parallel
29 shortening) and the stretching direction in the forebulge (where bulge-perpendicular
30 stretching induced by lithospheric outer arc extension operates) are nearly parallel in a belt-
31 perpendicular transect (Fig. 1). In addition, in the innermost portion of the foredeep, where
32 layer parallel shortening operates, the σ_2 is typically vertical and the σ_3 is positive,

Reviewer 1 comment 5

Unknown Author
24/06/2020 07:38

1 horizontal, and parallel to the trend of the belt (Tavani et al., 2015). Given the above, there
2 should be an area in between the inner portion of the foredeep and the peripheral bulge where
3 σ_1 becomes vertical and where σ_3 is still horizontal and parallel to the belt (Fig. 1a). This
4 scenario could explain the development of layer-perpendicular transverse extensional
5 structures, with transverse extensional faults or veins expected to develop where σ_3 is
6 positive. In this scenario, transverse joints occurring in this zone of localized tension could
7 only develop as cross-joints (e.g. Gross, 1993) of the longitudinal set formed in the forebulge.
8 This simplified model does not explain the documented occurrence of transverse joints in
9 areas where longitudinal joints do not occur or represent the cross-joint set (e.g. Zhao and
10 Jacobi, 1997; Quintà and Tavani, 2012). This framework does not admit a simple stress
11 permutation in the foredeep and requires a negative σ_3 connected to a foredeep-parallel
12 stretching component (Fig. 1b). Lithospheric bending of the foredeep, both along the
13 horizontal plane (e.g. Doglioni, 1995) and along the vertical plane parallel to the trench
14 (Quintà and Tavani, 2012), has been invoked as a process able to produce foredeep-parallel
15 stretching.

16 Continuous exposures across the entire foreland region of the eastern Pyrenees allows
17 investigation of the primary mechanism responsible for transverse joint development
18 described above. Tens to hundreds of meters long joints affect the sedimentary sequence of
19 the Ebro foredeep basin (Fig. 2a), and are found tilted within the frontal structures of the
20 Pyrenean belt (Fig. 2b). These pre-folding joints are exceptionally exposed and mappable
21 from orthophotos (Fig. 2c-f), from which they can be traced almost continuously from the
22 external portion of the foredeep until the thrust belt. We have remotely mapped 30059 joints
23 traces from the aforementioned orthophoto dataset and obtained their azimuthal distributions
24 across the study area. Subsequently, this extended lineament database has been used to
25 constrain [the](#) causative mechanism behind transverse jointing in the Ebro foredeep basin.

26

27 | **Geological Setting framework**

28 The study area is situated in the eastern Ebro foreland basin within an area connecting
29 the eastern Pyrenees with the Catalan Coastal Ranges (Fig. 3a). The Pyrenees is an EW-
30 striking orogenic system that formed as the Iberian and European plates collided from Late
31 Cretaceous to Miocene times (Roest and Srivastava, 1991; Rosenbaum et al., 2002; Muñoz,
32 | 1992, 2002), and constitutes [an](#) asymmetric, doubly vergent orogenic wedge above the

1 northward subduction of the Iberian lithosphere beneath the European plate (Chevrot et al.,
2 2018). As a result, the Ebro basin formed as a flexural foreland developed on the downgoing
3 Iberian plate at the southern margin of the chain (Beaumont et al., 2000). In the study area, to
4 the south of the Ebro Basin (Fig. 3a), the Catalan Coastal Ranges developed as a Paleogene
5 intraplate left-lateral transpressional system (López-Blanco, 2002; Santanach et al., 2011).
6 The low-displacement character of thrusts and the absence of an associated foredeep both
7 evidence the limited importance of this range. A series of NE-SW and NW-SE trending
8 extensional faults strike parallel and perpendicular to the Catalan Coastal Range respectively,
9 which are a result of the late Oligocene-Miocene opening of the NW Mediterranean basin
10 (Vegas, 1992; Sàbat et al., 1995; Granado et al., 2016a).

11 The study area where joint traces have been digitized is delimited to the north by the
12 frontal Pyrenean thrusts and by the Eocene Bellmunt anticline (Figs. 3a,b). This anticline
13 comprises the Paleocene to upper Eocene foredeep infill. Immediately to the south of the
14 anticline (i.e.< 5 km), this multilayer becomes sub-horizontal and thins southward where the
15 Paleozoic to Mesozoic foredeep floor gently rises up southward and becomes exposed (Fig.
16 3a). There, this pre-orogenic Paleozoic to Cenozoic succession is slightly tilted to the north by
17 uplift in the footwall of NW-SE striking Elate Oligocene to Neogene extensional faults.
18 Further to the southwest, this succession is affected by the Paleogene contractional structures
19 of the Catalan Coastal Ranges (Fig. 3b).

20 In the field, joints are constantly bedding-perpendicular, regardless of the bedding dip
21 (Fig. 2a,b), and they are characterized by the occurrence of either a single set (Fig. 2c) or by a
22 ladder pattern (Fig. 2d,e). In the latter case, the few E-W striking joints are almost
23 everywhere perpendicular to the N-S striking set and abut on it (Fig. 2e). This indicates that
24 E-W striking joints are cross-joints formed perpendicular to, and about synchronously with,
25 the N-S striking joint set.

Reviewer 1
Comment 3
&
Reviewer 2
Comment 5
Unknown Author
24/06/2020 07:41

28 Data and Methods

29 Joints have been digitized within the 16.4x49.2 km area displayed on Figure 3, on 25 and 50
30 cm/px orthophotos provided by the Spanish Instituto Geográfico Geográfico Nacional via the
31 PNOA (Plan Nacional de Ortofotografía Aérea) project (<https://pnoa.ign.es/>). The open
32 source geographical information system QGIS 3.4 has been used to manually digitize 30059

1 joint traces. A collection of these traces seen on orthophotos is provided in Figure 2c-f. Joints
2 have been digitized in Bartonian and, subordinately, in Lutetian and Priabonian sedimentary
3 rocks (Fig. 3c). The NE and SE portions of the study area are highly vegetated (Fig. 3d,e) and
4 only a few joint traces have been mapped there. Quaternary sediments unaffected by joints
5 crop out in the central portion of the study area (Fig. 3d).

6 Digitized traces have lengths ranging from 2 to 100 m, with an average of ~20 m (Fig.
7 3f). The frequency distribution of trace trend shows that the vast majority of the mapped
8 joints are approximately N-S striking (Fig. 3f). A second subordinate set corresponds to E-W
9 striking joints, which in the field occur as cross-joints (Fig. 2d). The frequency distribution of
10 trace trend is not symmetrical around these orthogonal sets, due to the presence of a third less
11 abundant set composed of NW-SE oriented joints (Fig. 2e,f). The NW-SE striking joints are
12 mostly seen in the southern portion of the study area, in exposures where the N-S striking set
13 is not occurring. Generally speaking, as previously mentioned above, exposures are
14 mostly frequently characterized by a single set (Fig. 32c,d). At a few many locations, the
15 dominant set is accompanied by associated cross-joints (Fig. 33d). Very rarely, two mutually
16 oblique sets occur in the same exposure (Fig. 2f).

17 In order to evaluate the variability of joint traces, the 16.4x49.2 km study area has
18 been divided into meshes of equilateral triangular elements with edge lengths of 1025m
19 (Mesh 1) and 1640m (Mesh 2). At each node, mean value and variance of trace trends has
20 been computed using a circular moving window with a radius of 1200m (Mesh 1) and 1900m
21 (Mesh 2). The radius of the circular moving window is set to these values for two reasons: 1)
22 it is two orders of magnitude longer than the average length of joints; 2) it is large enough to
23 ensure that most of the nodes have data number >20, as only nodes with data number > 20
24 have been analyzed. Since trace trends are circular data with an angle (α) over a period (π) in
25 agreement with Mardia (1975) we used equations 1 to 4 to derive at each node the circular
26 mean value (Mv_{π}), the circular variance (V_{π}) and the resultant length (R_{π} ; $V_{\pi} = 1-R_{\pi}$), the
27 latter spanning from 0 (unclustered distribution) to 1 (perfectly clustered distribution). In the
28 presence of cross-orthogonal joint sets, it is also useful using a period of $\pi/2$, thus modifying
29 Mardia's equations and introducing the $Mv_{\pi/2}$ and $R_{\pi/2}$ parameters, which are computed using
30 Equations 5 to 8.

31

Reviewer 1
Comment 7

Unknown Author
24/06/2020 07:39

$$1 \quad C_{\pi} = \frac{\sum_{i=1}^n \cos(2\alpha_i)}{n} \quad (1) ; \quad S_{\pi} = \frac{\sum_{i=1}^n \sin(2\alpha_i)}{n} \quad (2) ; \quad V_{\pi} = 1 - R_{\pi} = 1 - \sqrt{C_{\pi}^2 + S_{\pi}^2} \quad (3) ; \quad Mv_{\pi} = \frac{\operatorname{Arctan}(S_{\pi}/C_{\pi})}{2} \quad (4)$$

$$C_{\pi/2} = \frac{\sum_{i=1}^n \cos(4\alpha_i)}{n} \quad (5) ; \quad S_{\pi/2} = \frac{\sum_{i=1}^n \sin(4\alpha_i)}{n} \quad (6) ; \quad V_{\pi/2} = 1 - R_{\pi/2} = 1 - \sqrt{C_{\pi/2}^2 + S_{\pi/2}^2} \quad (7) ; \quad Mv_{\pi/2} = \frac{\operatorname{Arctan}(S_{\pi/2}/C_{\pi/2})}{4} \quad (8)$$

2

3 By using these four parameters together, instead for example of the classical k-means
 4 clustering analysis, it is possible to derive important considerations on the distribution of
 5 polymodal distributions in which two mutually orthogonal sets do occur, as illustrated in
 6 Figure 4. We compare the Mv and the R parameters computed using the π and $\pi/2$ periods. In
 7 the first example two parallel traces are analyzed, resulting in $Mv_{\pi/2} = Mv_{\pi}$, and $R_{\pi/2} = R_{\pi} = 1$
 8 (i.e. circular variance = 0). When data dispersion is slightly increased (Example 2), $Mv_{\pi/2}$ is
 9 still equal to Mv_{π} , whereas $R_{\pi/2}$ decreases faster than R_{π} . Further increase of data dispersion
 10 (Example 3), in an asymmetric distribution (i.e. non-orthogonal sets), causes additional
 11 decrease of $R_{\pi/2}$ with respect to R_{π} , and slight divergence between $Mv_{\pi/2}$ and Mv_{π} . In the
 12 presence of a cross-orthogonal subset, the statistical usefulness of $R_{\pi/2}$ becomes evident, as
 13 illustrated in Example 4. In this case, R_{π} rapidly approaches zero, suggesting high dispersion
 14 (i.e. unrepresentative Mv_{π}), whereas $R_{\pi/2}$ is essentially unaffected with respect to Example 2,
 15 indicating low dispersion and a representative $Mv_{\pi/2}$. However, the use of the $\pi/2$ period only
 16 returns results in the 0 to $\pi/2$ range, so that NW-SE trending traces result in a NE-SW
 17 trending mean value ($Mv_{\pi/2}$), as shown in the Example 5. In summary, Mv_{π} is useful to derive
 18 the mean direction, whereas $R_{\pi/2}$ and R_{π} should be used in conjunction to discriminate
 19 between populations in which oblique sets occur ($R_{\pi/2} < R_{\pi}$) from those in which two
 20 perpendicular sets occur ($R_{\pi/2} > R_{\pi}$).

21

22 Results

23 Figure 5 displays attribute maps generated from Mesh 1 and Mesh 2 using the trace
 24 orientation parameters described above. Both Mesh 1 and Mesh 2 have $R_{\pi} > 0.5$ across almost
 25 the entirety of the study area, with the only exception being in the NW corner of the study
 26 area. For $R_{\pi/2}$, in addition to the NW corner, the central portion of the study area has $R_{\pi/2} <$
 27 0.5. Noteworthy differences between R_{π} and $R_{\pi/2}$ occur: (1) in the NW corner ($R_{\pi} \ll R_{\pi/2}$) and
 28 (2) in the central area ($R_{\pi} \gg R_{\pi/2}$). The first area corresponds to a vegetated folded and faulted
 29 area-zone (Fig 3b-e). Consequently, we consider the dataset poorly reliable in this location. In
 30 the central portion of the study area, the difference between R_{π} and $R_{\pi/2}$ (which increases as

1 data dispersion increases) is less pronounced in Mesh 1 than Mesh 2. Thus, data dispersion
2 increases with increasing the search window size (1200m for Mesh 1 and 1900m for Mesh 2),
3 evidencing that joint orientation is changing in this area. In the rest of the analyzed foreland,
4 $R_{\pi/2}$ has values similar to R_π , indicating approximately unimodal data distribution within this
5 region, and poor spatial organization of the longitudinal cross-joints.

6 Distribution of Mv_π relates to the prevalence of NS-striking joints in the northern and
7 central portion of the study area. Towards the south, patches characterized by both N-S and
8 NW-SE-striking joints occur. High values of R_π and $R_{\pi/2}$ are characteristic of such subareas,
9 which as previously mentioned, is indicative of unimodal joint trace distributions.

10

11 Discussion

12 Remotely sensed and mapped joint traces in the eastern portion of the Pyrenees-Ebro
13 system show systematic distributions of azimuthal orientations. In the frontal portion of the
14 belt and within the foredeep, joints are mostly transverse (i.e. N-S-striking), with limited
15 occurrence of E-W-striking longitudinal cross-joints. Approaching the southern border of the
16 foredeep, joints exhibit both N-S and NW-SE orientations where the pre-Cenozoic floor of
17 the foredeep is exposed. Joints affect the Lutetian to Priabonian foredeep infill, and are found
18 tilted together with strata within the Bellmunt anticline (Fig. 2b), which is Priabonian in age
19 (Burbank et al., 1992). Given the above, the timing of jointing in the area must have taken
20 place before during or before the Priabonian. Evidencing this proposed framework, there are no
21 systematic and pervasive joints affecting Quaternary sediments (Fig. 3), while Oligo-Mio-
22 Pliocene sediments are not present in the rock record of the studied area. The occurrence of
23 the N-S striking joints within the Ebro foredeep is documented also to the west of the study
24 area (e.g. Turner and Hancock, 1990), where joint emplacement affects up to the Miocene
25 (Arlegui and Simon, 2001). Transverse joints, striking approximately NNE-SSW occur also
26 to the SW in the Bartonian to Priabonian strata cropping out at the boundary between the
27 Ebro basin and the Catalan Coastal Ranges (Alsaker et al., 1996). These data indicate that
28 transverse joints systematically developed in the foredeep basin of the E-W oriented
29 Pyrenean belt. Locally, the process of transverse jointing occurred until the early Miocene
30 (i.e. until the end of mountain building). Also, pre-thrusting transverse extensional faults of
31 upper Paleocene to lower Eocene age occur a few tens of km to the NE of the study area
32 (Carrillo et al., 2020), being presently incorporated into the Pyrenean belt. Thus, we conclude

1 that foredeep-parallel extension has occurred in the foredeep of the Pyrenean belt since the
2 Paleocene and until the end of convergence. Transverse joints documented in this work
3 clearly represent foredeep-related structures, which can develop by (i) N-S oriented layer-
4 parallel shortening (LPS) or (ii) E-W oriented along foredeep stretching –(Tavani et al.,
5 2015). LPS is to be excluded, as the state of stress in this case would include a positive
6 minimum stress (Fig. 1). In agreement, LPS-related extensional structures can form only due
7 to fluid pressure contribution and they include mm- to cm-long fractures filled with calcite
8 (which is removed from pressure solution seams, Fig. 1; Tavani et al., 2015 and references
9 therein). The type (joints with no calcite infill) and size (tens of m-long) of transverse
10 extensional structures described here are incompatible with the layer-parallel shortening
11 mechanism.

Reviewer 1
Comment 1

Unknown Author
24/06/2020 07:39

12 The relatively constant orientation of joints along the strike of the foredeep, the
13 occurrence of appreciable dispersion at the outer border of the foredeep, and the remarkably
14 poor abundance of longitudinal joints allow us to derive two major conclusions:

15 (1) The almost linear trend of the eastern Pyrenees facilitates the exclusion of planar arching
16 (e.g. Doglioni, 1995; Zhao and Jacobi, 1997) as the causative process for generating
17 foredeep-parallel stretching (i.e. required to establish the negative σ_3 responsible for
18 transverse jointing). Arching along the vertical plane parallel to the trench (Quintà and
19 Tavani, 2012) represents instead a viable mechanism for generating along-foredeep
20 stretching. This is analogous, albeit at a larger scale to the process of release faulting
21 described by Destro (1995). The basic concept behind this mechanism is the following: when
22 a straight line joining two fixed points - the tips of a fault in the case of Destro (1995) or the
23 edges of the foredeep in the case of Quintà and Tavani (2012) – becomes an arch, there is
24 stretching (Fig. 1b), which causes extensional stress parallel to the direction of elongation. In
25 essence, this mechanism is expected to operate in any doubly plunging foredeep, particularly
26 at its lateral edges, and requires a laterally decreasing depth of the foredeep, which is
27 confirmed by the westward plunge of the foredeep basin, such as in the study area (Fig. 3a).

Reviewer 2
Comment 2

Unknown Author
24/06/2020 07:47

28 (2) Extension in the peripheral bulge, which is documented from many active and fossil
29 foredeep basins (e.g. Bradley and Kidd, 1991; Ranero et al., 2003; Tavani et al., 2015;
30 Granado et al., 2016b), including the lower Eocene foredeep basin presently incorporated into
31 the Pyrenees (e.g. Martinez et al., 1989; Pujadas et al., 1989) appears to be weakly influential
32 at the southern border of the study area (i.e. the upper Eocene peripheral bulge). Indeed, the

1 observed longitudinal joints are characteristically subbordered, forming locally as cross-joints
2 to the identified transverse set within the study area (Fig. 2d). The transverse set becomes less
3 organized at the southern margin of the foredeep, where patches of N-S and NW-SE
4 dominated domains do occur. This evidences the absence of a major forebulge-perpendicular
5 extension capable of systematically reorienting σ_3 at the external foredeep edge.

6

7 **Conclusions**

8 Analysis of remotely sensed and mapped joints in the eastern Pyrenees and in the
9 adjacent Ebro foreland basin indicates that the emplacement of the dominant joint set within
10 the area, which strikes perpendicular to the trend of the foredeep occurred prior to folding
11 and developed in response to along-strike stretching caused by the plunging shape of the
12 foredeep. Joints developed in response to flexuring of the lithosphere at the peripheral bulge
13 do not occur in the area, suggesting that this mechanism has limited relevance to the observed
14 joint system. This is confirmed by the variability of joint orientations observed at the
15 foredeep external edge, negating the occurrence of a major forebulge-perpendicular extension
16 able to systematically orient the stress field at the foredeep edge.

17

18

19

20

21 **Data availability**

22 | Digitized traces in shapefile format [and bedding and joint data in csv format](#) are in the
23 supplementary materials

24

25 **Author contributions**

26 | ST, PG, AC, TS, [JMC](#), and JAM contributed equally to the elaboration of the manuscript.

27

28 **Competing interests**

29 The authors declare that they have no conflict of interest.

30

31 **Acknowledgements**

1 | We thank Eric Salomon and an anonymous referee for useful suggestions. The Institut de
2 Recerca Geomodels and the Geodinàmica i Anàlisi de Conques research group
3 (2014SGR467SGR) acknowledges financial support from the Agència de Gestió d'Ajuts
4 Universitaris i de Recerca (AGAUR) and the Secretaria d'Universitats i Recerca del
5 Departament d'Economia i Coneixement de la Generalitat de Catalunya. [Financial support](#)
6 [form projects CGL2017-87631-P and PGC2018-093903-B-C22 from Ministerio de Ciencia,](#)
7 [Innovación y Universidades/Agencia Estatal de Investigación/Fondo Europeo de Desarrollo](#)
8 [Regional, Unión Europea is also acknowledged.](#)

9

10 References

11 Alsaker, E., Gabrielsen, R. H., and Roca, E.: The significance of the fracture pattern of the
12 Late-Eocene Montserrat fan-delta, Catalan Coastal Ranges (NE Spain),
13 Tectonophysics, 266, 465-491, [https://doi.org/10.1016/S0040-1951\(96\)00239-9](https://doi.org/10.1016/S0040-1951(96)00239-9), 1996

14 Arlegui, L., and Simón, J. L.: Geometry and distribution of regional joint sets in a non-
15 homogeneous stress field: case study in the Ebro basin (Spain), Journal of Structural
16 Geology, 23, 297-313, [https://doi.org/10.1016/S0191-8141\(00\)00097-3](https://doi.org/10.1016/S0191-8141(00)00097-3), 2001

17 Barr, D., Savory, K.E., Fowler, S.R., Arman, K., and McGarry, J.P.: Pre-development
18 fracture modelling in the Clair field, west of Shetland, Geol. Soc. Lond. Special
19 Publication, 270, 205-225, <https://doi.org/10.1144/GSL.SP.2007.270.01.14>, 2007

20 Basa, A., Ahmed, F., Bhattacharyya, K., and Roy, A.: Evolution and characterization of
21 fracture patterns: Insights from multi-scale analysis of the Buxa dolomite in the Siang
22 Valley, Arunachal Lesser Himalayan fold-thrust belt. Journal of Structural Geology,
23 123, 54-66, <https://doi.org/10.1016/j.jsg.2019.03.004>, 2019

24 Beaumont, C., Muñoz, J. A., Hamilton, J., and Fullsack, P.: Factors controlling the Alpine
25 evolution of the central Pyrenees inferred from a comparison of observations and
26 geodynamical models, Journal of Geophysical Research: Solid Earth, 105, 8121-
27 8145, <https://doi.org/10.1029/1999JB900390>, 2000

28 Beaudoin, N., Lacombe, O., David, M-E, and Koehn, D.: Does stress transmission in forelands
29 depend on structural style?. Distinctive stress magnitudes during Sevier thin-skinned
30 and Laramide thick-skinned layer-parallel shortening in the Bighorn Basin (USA)

1 revealed by stylolite and calcite twinning paleopiezometry, *Terra Nova*, <https://doi.org/10.1111/ter.12451>, 2020

2

3 Berkowitz, B., Bear, J., and Braester, C.: Continuum models for contaminant transport in
4 fractured porous formations, *Water Resour. Res.*, 24, 1225-1236,
5 <https://doi.org/10.1029/WR024i008p01225>, 1988

6 Billi, A., and Salvini, F.: Development of systematic joints in response to flexure-related fibre
7 stress in flexed foreland plates: the Apulian forebulge case history, Italy, *Journal of*
8 *Geodynamics*, 36, 523-536, [https://doi.org/10.1016/S0264-3707\(03\)00086-3](https://doi.org/10.1016/S0264-3707(03)00086-3), 2003

9 Bradley, D. C., and Kidd, W. S. F.: Flexural extension of the upper continental crust in
10 collisional foredeeps, *Geological Society of America Bulletin*, 103, 1416-1438, [https://doi.org/10.1130/0016-7606\(1991\)103<1416:FEOTUC>2.3.CO;2](https://doi.org/10.1130/0016-7606(1991)103<1416:FEOTUC>2.3.CO;2), 1991

11

12 Branellec, M., Callot, J. P., Nivière, B., and Ringenbach J. C.: The fracture network, a proxy
13 for mesoscale deformation: Constraints on layer parallel shortening history from the
14 Malargüe fold and thrust belt, Argentina, *Tectonics*, 34, 623-647,
15 <https://doi.org/10.1002/2014TC003738>, 2015

16 Burbank, D. W., Puigdefàbregas, C., and Muñoz, J. A.: The chronology of the Eocene
17 tectonic and stratigraphic development of the eastern Pyrenean foreland basin,
18 northeast Spain, *Geological Society of America Bulletin*, 104, 1101-1120,
19 [http://doi.org/10.1130/0016-7606\(1992\)104<1101:TCOTET>2.3.CO;2](http://doi.org/10.1130/0016-7606(1992)104<1101:TCOTET>2.3.CO;2), 1992

20 Carrillo, E., Guinea, A., Casas, A., Rivero, L., Cox, N., and Vázquez-Taset, Y. M.: Tectono-
21 sedimentary evolution of transverse extensional faults in a foreland basin: Response to
22 changes in tectonic plate processes. *Basin Research*, <https://doi.org/10.1111/bre.12434>,
23 2020

24 Chevrot, S., Sylvander, M., Díaz, J., Martin, R., Mouthereau, F., Manatschal, G., Masini, E.,
25 Calassou, S., Grimaud, F., Pauchet, H., and Ruiz, M.: The non-cylindrical crustal
26 architecture of the Pyrenees, *Scientific Reports*, 8, 9591,
27 <https://doi.org/10.1038/s41598-018-27889-x>, 2018

28 Destro, N.: Release fault: A variety of cross fault in linked extensional fault systems, in the
29 Sergipe-Alagoas Basin, NE Brazil, *Journal of Structural Geology*, 17, 615-629, [https://doi.org/10.1016/0191-8141\(94\)00088-H](https://doi.org/10.1016/0191-8141(94)00088-H), 1995

30

1 Dietrich, D.: Fold-axis parallel extension in an arcuate fold-and thrust belt: the case of the
2 Helvetic nappes. *Tectonophysics*, 170, 183-212, [https://doi.org/10.1016/0040-1951\(89\)90271-0](https://doi.org/10.1016/0040-1951(89)90271-0), 1989

4 Doglioni, C.: Geological remarks on the relationships between extension and convergent
5 geodynamic settings, *Tectonophysics*, 252, 253-267. [https://doi.org/10.1016/0040-1951\(95\)00087-9](https://doi.org/10.1016/0040-1951(95)00087-9), 1995

7 Dunne, W. M., and North, C. P.: Orthogonal fracture systems at the limits of thrusting: an
8 example from southwestern Wales, *Journal of Structural Geology*, 12, 207-215, [https://doi.org/10.1016/0191-8141\(90\)90005-J](https://doi.org/10.1016/0191-8141(90)90005-J), 1990

10 Engelder, T., Lash, G.G., and Uzcategui, R.: Joint sets that enhance production from Middle-
11 Upper Devonian gas shales of the Appalachian basin, *AAPG Bull.*, 93, 857-889,
12 <https://doi.org/10.1306/03230908032>, 2009

13 Giuffrida, A., La Bruna, V., Castelluccio, P., Panza, E., Rustichelli, A., Tondi, E., Giorgioni,
14 M., Agosta, F.: Fracture simulation parameters of fractured reservoirs: Analogy with
15 outcropping carbonates of the Inner Apulian Platform, southern Italy, *Journal of*
16 *Structural Geology*, 123, 18-41, <https://doi.org/10.1016/j.jsg.2019.02.007>, 2019

17 Granado, P., Urgeles, R., Sábat, F., Albert-Villanueva, E., Roca, E.. Muñoz, J.A., Mazzucca,
18 N., and Gambini, R.: Geodynamical framework and hydrocarbon plays of a salt giant:
19 the North Western Mediterranean Basin, *Petroleum Geoscience*, 22, 309-321,
20 <https://doi.org/10.1306/0323090803210.1144/petgeo2015-084>, 2016a

21 Granado, P., Thöny, W., Carrera, N., Gratzer, O., Strauss, P. and Muñoz, J.A.: Basement-
22 involved reactivation in fold and thrust belts: the Alpine-Carpathian Junction (Austria),
23 *Geological Magazine*, 153, 1100-1135, : <https://doi.org/10.1017/S0016756816000066>,
24 2016b

25 Gross, M. R.: The origin and spacing of cross joints: examples from the Monterey
26 Formation, Santa Barbara Coastline, California, *Journal of Structural Geology*, 15,
27 737-751, [https://doi.org/10.1016/0191-8141\(93\)90059-J](https://doi.org/10.1016/0191-8141(93)90059-J), 1993

28 Haffen, S., Géraud, Y., Diraison, M., and Dezayes, C.: Determination of fluid-flow zones in a
29 geothermal sandstone reservoir using thermal conductivity and temperature logs,
30 *Geothermics*, 46, 32-41, <https://doi.org/10.1016/j.geothermics.2012.11.001>, 2013

1 Iding, M., and Ringrose, P.: Evaluating the impact of fractures on the performance of the In
2 Salah CO₂ storage site, International Journal of Greenhouse Gas Control, 4, 242-248,
3 <https://doi.org/10.1016/j.ijggc.2009.10.016>, 2010

4 Lash, G.G., and Engelder, T.: Jointing within the outer arc of a forebulge at the onset of the
5 Alleghanian Orogeny, Journal of Structural Geology, 29, 774-786,
6 <https://doi.org/10.1016/j.jsg.2006.12.002>, 2007

7 Laubach, S. E., Lander, R. H., Criscenti, L. J., Anovitz, L. M., Urai, J. L., Polleyea, R. M.,
8 Hooker, J. N., Narr, W., Evans, M. A., Kerisit, S. N., Olson, S. N., Dewers, T.,
9 Fisher, D., Bodnar, R., Evans, B., Dove, P., Bonnell, L. M., Marder, M. P., Pyrak-
10 Nolte, M. P.: The role of chemistry in fracture pattern development and opportunities
11 to advance interpretations of geological materials. Reviews of Geophysics, 57, 1065–
12 1111, <https://doi.org/10.1029/2019RG000671>, 2019

13 Lemiszki, P.J., Landes, J.D., and Hatcher, R.D.: Controls on hinge-parallel extension
14 fracturing in single-layer tangential-longitudinal strain folds, Journal of Geophysical
15 Research: Solid Earth, 99, 22027-22041, <https://doi.org/10.1029/94JB01853>, 1994

16 López-Blanco, M.: Sedimentary response to thrusting and fold growing on the SE margin of
17 the Ebro basin (Paleogene, NE Spain), Sedimentary Geology, 146, 133-154,
18 [https://doi.org/10.1016/S0037-0738\(01\)00170-1](https://doi.org/10.1016/S0037-0738(01)00170-1), 2002

19 Mardia, K.V.: Statistics of directional data. Journal of the Royal Statistical Society. Series B
20 (Methodological), 37, 349-393, 1975

21 Martinelli, M., Bistacchi, A., Balsamo, F., and Meda, M.: Late Oligocene to Pliocene
22 extension in the Maltese Islands and implications for geodynamics of the Pantelleria
23 Rift and Pelagian Platform, Tectonics, 38, 3394-3415,
24 <https://doi.org/10.1029/2019TC005627>, 2019

25 Martinez, A., Verges, J., Clavell, E., and Kennedy, J.: Stratigraphic framework of the thrust
26 geometry and structural inversion in the southeastern Pyrenees: La Garrotxa Area,
27 Geodinamica Acta, 3, 185-194, <https://doi.org/10.1080/09853111.1989.11105185>,
28 1989

29 Masciopinto, C., and Palmiotta, D.: Flow and transport in fractured aquifers: new conceptual
30 models based on field measurements, Transport in Porous Media, 96, 117-133, <https://doi.org/10.1007/s11242-012-0077-y>, 2013

1 Muñoz, J.A.: Evolution of a continental collision belt: ECORS-Pyrenees crustal balanced
2 cross-section. In: McClay (Ed.), *Thrust Tectonics*. Chapman & Hall, London, 235-246,
3 1992

4 Muñoz, J. A.: The Pyrenees. In: *The Geology of Spain*, W. Gibbons and M. T. Moreno (eds.),
5 pp. 370-385, Geological Society, London, U. K., 2002

6 Murray, G. H., Jr.: Quantitative fracture study - Sanish pool, McKenzie County, North
7 Dakota, *AAPG Bull.*, 52, 57-65, 1968

8 Parés, J. M., van der Pluijm, B. A., and Dinarès-Turell, J.: Evolution of magnetic fabrics
9 during incipient deformation of mudrocks (Pyrenees, northern Spain), *Tectonophysics*,
10 307, 1-14, [https://doi.org/10.1016/S0040-1951\(99\)00115-8](https://doi.org/10.1016/S0040-1951(99)00115-8), 1999

11 | Pujadas, J., Casas, J.M., Muñoz, J.A., and Sábat, F.: Thrust tectonics and paleogene
12 syntectonics sedimentation in the Empordà area, southeastern Pyrenees, *Geodinamica
Acta*, 3, 195-206, <https://doi.org/10.1080/09853111.1989.11105186>, 1989

14 | Questiaux, J., M., Couples, G.D., and Ruby, N.: Fractured reservoirs with fracture corridors,
15 Geophysical Prospecting, 58, 279-295, [https://doi.org/10.1111/j.1365-
16 2478.2009.00810.x](https://doi.org/10.1111/j.1365-2478.2009.00810.x), 2010

17 Quintà, A., and S. Tavani: The foreland deformation in the south-western Basque–Cantabrian
18 Belt (Spain), *Tectonophysics*, 576, 4-19. <https://doi.org/10.1016/j.tecto.2012.02.015>,
19 2012

20 Ramsay, J.G.: *Folding and Fracturing of Rocks*. McGraw-Hill Book Company, Inc. New
21 York. 568Pp, 1967

22 Ranero, C. R., Morgan, J. P., McIntosh, K., and Reichert, C.: Bending-related faulting and
23 mantle serpentinization at the Middle America trench, *Nature*, 425, 367-373,
24 <https://doi.org/10.1038/nature01961>, 2003

25 Roest, W. R., and Srivastava, S. P.: Kinematics of the plate boundaries between Eurasia,
26 Iberia, and Africa in the North Atlantic from the Late Cretaceous to the present,
27 *Geology*, 19, 613-616, [https://doi.org/10.1130/0091-
28 7613\(1991\)019<0613:KOTPBB>2.3.CO;2](https://doi.org/10.1130/0091-7613(1991)019<0613:KOTPBB>2.3.CO;2), 1991

29 Rosenbaum, G., Lister, G. S., and Duboz, C.: Reconstruction of the tectonic evolution of the
30 western Mediterranean since the Oligocene, *Journal of the Virtual Explorer*, 8, 107-
31 130, 2002

1 Sàbat, F., Roca, E., Muñoz, J.A., Vergés, J., Sans, M., Masana, E., Santanach, P., Estévez,
2 A., and Santisteban, C.: Role of extension and compression in the evolution of the
3 eastern margin of Iberia: the ESCI- València Trough seismic profile, *Rev. Soc. Esp.*
4 *Geol.*, 8, 431-448, 1995

5 Santanach, P., Casas, J.M., Gratacós, O., Liesa, M., Muñoz, J.A., and Sàbat, F.: Variscan and
6 Alpine structure of the hills of Barcelona: geology in an urban area, *Journal of Iberian*
7 *Geology*, 37, 121-136, https://doi.org/10.5209/rev_JIGE.2011.v37.n2.2, 2011

8 Tavani, S., Storti, F., Lacombe, O., Corradetti, A., Muñoz, J. A., and Mazzoli, S.: A review of
9 deformation pattern templates in foreland basin systems and fold-and-thrust belts:
10 Implications for the state of stress in the frontal regions of thrust wedges. *Earth-*
11 *Science Reviews*, 141, 82-104, <https://doi.org/10.1016/j.earscirev.2014.11.013>, 2015

12 Tavani, S., Corradetti, A., De Matteis, M., Iannace, A., Mazzoli, S., Castelluccio, A.,
13 Spanos, D., and Parente, M.: Early-orogenic deformation in the Ionian zone of the
14 Hellenides: Effects of slab retreat and arching on syn-orogenic stress evolution. *Journal*
15 *of Structural Geology*, 124, 168-181, <https://doi.org/10.1016/j.jsg.2019.04.012>, 2019

16 Tavarnelli, E., and Peacock, D. C.: From extension to contraction in syn-orogenic foredeep
17 basins: the Contessa section, Umbria-Marche Apennines, Italy, *Terra Nova*, 11, 55-60,
18 <https://doi.org/10.1046/j.1365-3121.1999.00225.x>, 1999

19 Turner, J. P., and Hancock, P. L.: Relationships between thrusting and joint systems in the
20 Jaca thrust-top basin, Spanish Pyrenees. *Journal of structural geology*, 12(2), 217-226,
21 [https://doi.org/10.1016/0191-8141\(90\)90006-K](https://doi.org/10.1016/0191-8141(90)90006-K), 1990

22 Vegas, R.: The Valencia Trough and the origin of the western Mediterranean basins.
23 *Tectonophysics*, 203, 249-261, 1992

24 Vidal, J., Genter, A., and Chopin, F.: Permeable fracture zones in the hard rocks of the
25 geothermal reservoir at Rittershoffen, France, *Journal of Geophysical Research: Solid*
26 *Earth*, 122, 4864- 4887, <https://doi.org/10.1002/2017JB014331>, 2017

27 Whitaker, A. E., and Engelder, T.: Plate-scale stress fields driving the tectonic evolution of
28 the central Ouachita salient, Oklahoma and Arkansas, *Geological Society of America*
29 *Bulletin*, 118, 710-723, <https://doi.org/10.1130/B25780.1>, 2006

1 Zhao, M., and Jacobi, R.D.: Formation of regional cross-fold joints in the northern
2 Appalachian Plateau, Journal of Structural Geology, 19, 817-834,
3 [https://doi.org/10.1016/S0191-8141\(97\)00009-6](https://doi.org/10.1016/S0191-8141(97)00009-6), 1997

4

1 **Captions**

2 Figure 1

3 Scheme showing the architecture of a foreland fold-and-thrust belt and adjacent foredeep
4 basin, with syn-orogenic fracture patterns in the different structural domains of the orogenic
5 system. (A) The foredeep state of stress is governed by the permutation between the state of
6 stress in the layer-parallel shortening and peripheral bulge domains. (B) The foredeep state of
7 stress is controlled by the along-strike stretching of the foredeep.

8

9 Figure 2

10 Examples of pre-folding joints within the studied area. (A) N-S striking joint with plumose
11 structures in the foredeep sediments (42°02'39.7"N; 2°13'54.9"E). (B) Tilted N-S and E-W
12 striking joints in the southern limb of the Bellmunt anticline. with the red arrow indicating an
13 E-W striking joint abutting on a N-S striking joint -(42°05'39"N; 2°17'41.5"E). The density
14 contours of poles to bedding and joints (in their present day orientation and after unfolding)
15 refer to data collected in the Bellmunt anticline area. (C to F) Examples of joints seen on
16 orthophotos. (C) Transverse joints. (D) N-S striking transverse joints with subordinate E-W
17 striking cross-orthogonal joints. (E) NW-SE striking joints. (F) Rare example of multiple
18 oblique sets occurring at the same exposure. Orthophotos are available from the Spanish
19 Instituto Geográfico Nacional (<https://pnoa.ign.es/>).

20

21 Figure 3

22 (A) Simplified geological map of the western Pyrenees and Catalan Coastal Ranges (based on
23 the Geological Map of Catalunya scale 1:250'000; <https://www.icgc.cat/en/Downloads>), with
24 N-S geological cross-section (modified from Parés et al., 1999). (B) Detailed geological map
25 of the study area, with digitized joints (C). (D) Orthophoto (<https://pnoa.ign.es/>) of the study
26 area, with digitized joints (E). (F) Frequency distribution of joint traces trend and length.

27

28 Figure 4

29 Examples of joint patterns and resultant Mv and R parameters calculated for the π and $\pi/2$
30 periods. For the five examples, we show the map view of the joints, the azimuthal frequency,
31 and the sin-cos coordinates of the resultant values of Mv and R. Note that the distance from
32 the center is proportional to R.

Reviewer 2
Comment 7

Unknown Author
24/06/2020 07:49

1

2 Figure 5

3 Results of circular statistics analysis for both Meshes 1 and 2. Length of traces of Mv_π is
4 proportional to R_π . [Color code refers to \$R_\pi\$ and \$R_{\pi 2}\$](#) , whereas the orientation of traces is the
5 [\$Mv_\pi\$](#) . See text for details.

6

7

8

Reviewer 2
Comment 11

Unknown Author
24/06/2020 07:51

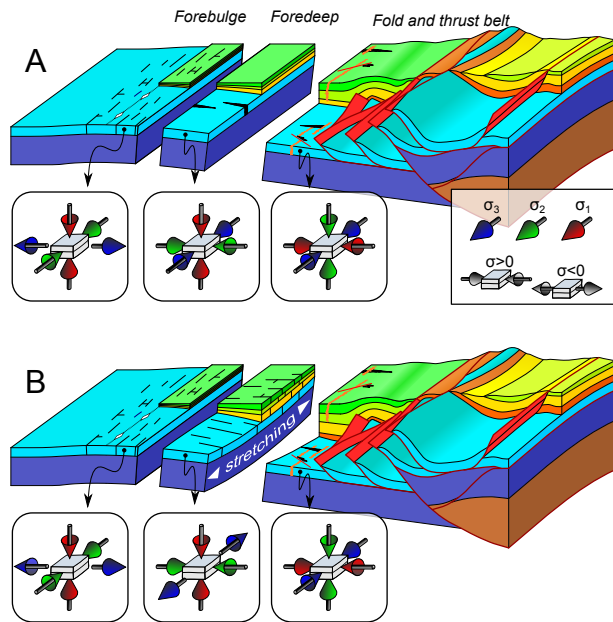


Figure 1 (Single column)

Scheme showing the architecture of a foreland fold-and-thrust belt and adjacent foredeep basin, with syn-orogenic fracture patterns in the different structural domains of the orogenic system. (A) The foredeep state of stress is governed by the permutation between the state of stress in the layer-parallel shortening and peripheral bulge domains. (B) The foredeep state of stress is controlled by the along-strike stretching of the foredeep.

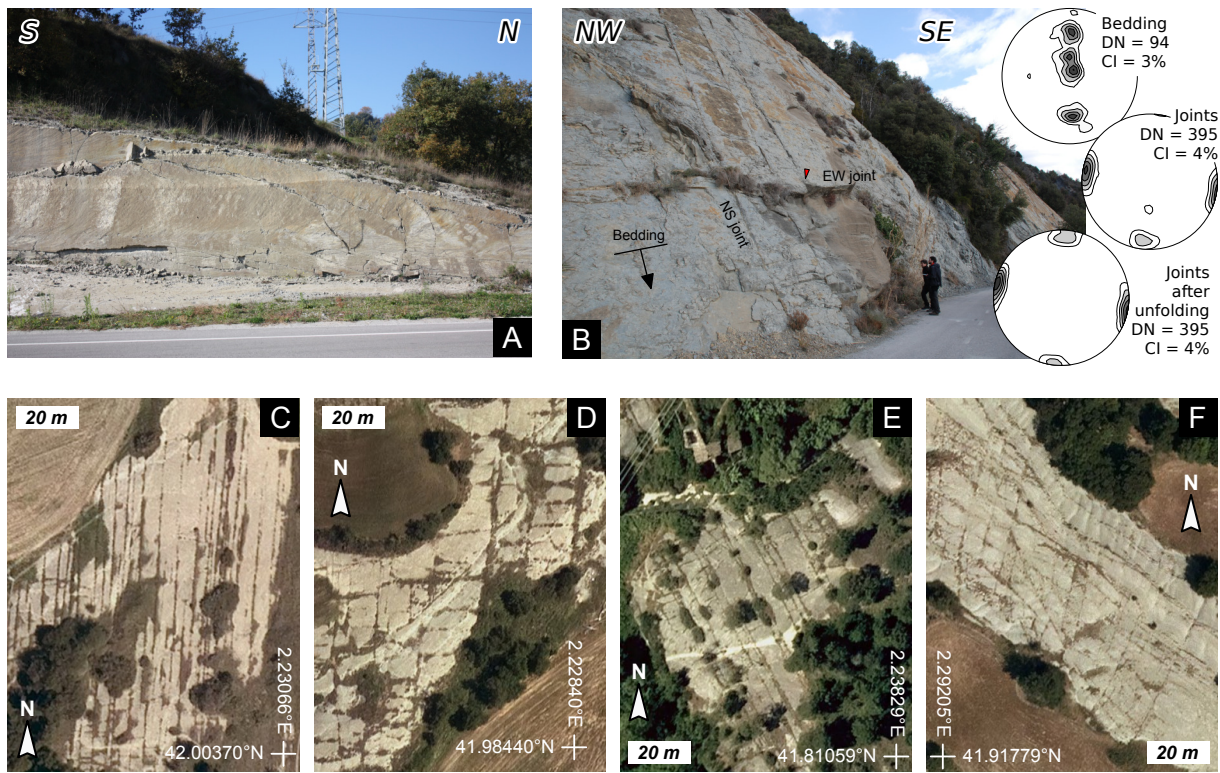


Figure 2 (Double column)

Examples of pre-folding joints within the studied area. (A) N-S striking joint with plumose structures in the foredeep sediments ($42^{\circ}02'39.7''N$; $2^{\circ}13'54.9''E$). (B) Tilted N-S and E-W striking joints in the southern limb of the Bellmunt anticline, with the red arrow indicating an E-W striking joint abutting on a N-S striking joint ($42^{\circ}05'39''N$; $2^{\circ}17'41.5''E$). The density contour of poles to bedding and joints (in their present day orientation and after unfolding) refer to data collected in the Bellmunt anticline area. (C to F) Examples of joints seen on orthophotos. (C) Transverse joints. (D) N-S striking transverse joints with subordinate E-W striking cross-orthogonal joints. (E) NW-SE striking joints. (F) Rare example of multiple oblique sets occurring at the same exposure. Orthophotos are available from the Spanish Instituto Geográfico Nacional (<https://pnoa.ign.es/>).

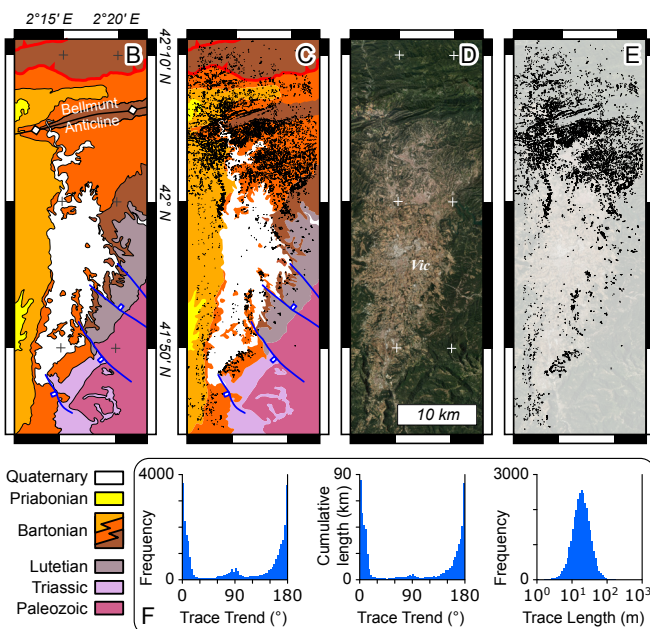
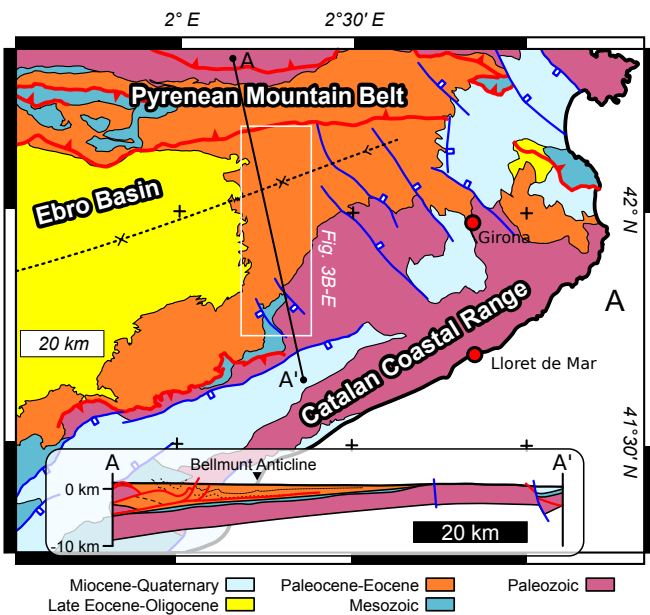


Figure 3 (Single column)

(A) Simplified geological map of the western Pyrenees and Catalan Coastal Ranges (based on the Geological Map of Catalonia scale 1:250'000; <https://www.icgc.cat/en/Downloads>), with N-S geological cross-section (modified from Parés et al., 1999). (B) Detailed geological map of the study area, with digitized joints (C). (D) Orthophoto (<https://pnoa.ign.es/>) of the study area, with digitized joints (E). (F) Frequency distribution of joint traces trend and length.

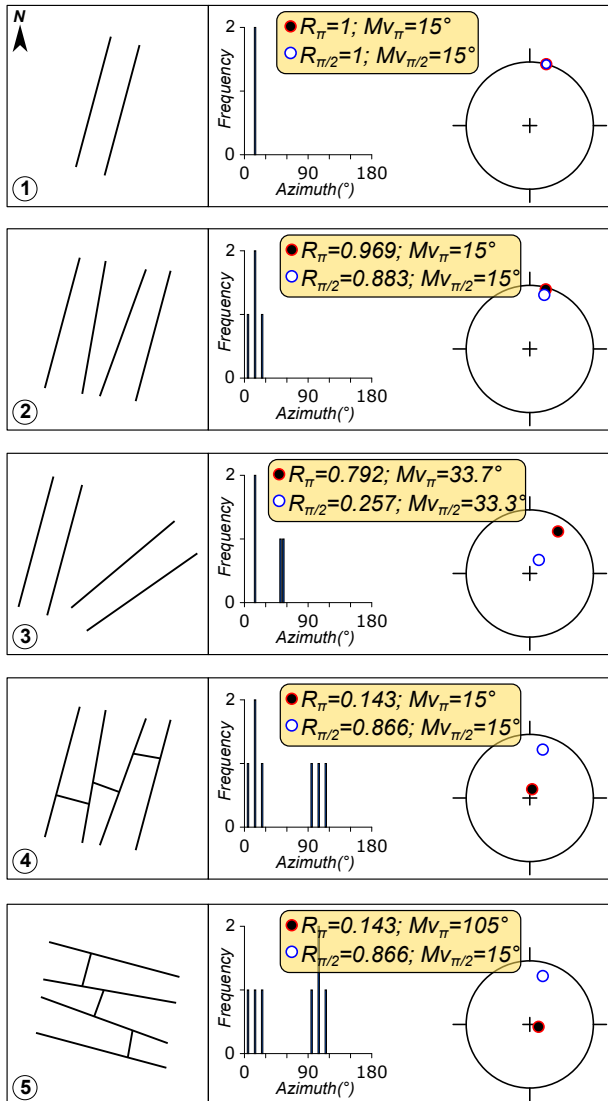


Figure 4 (Single column)

Examples of joint patterns and resultant Mv and R parameters calculated for the π and $\pi/2$ periods. For the five examples, we show the map view of the joints, the azimuthal frequency, and the sin-cos coordinates of the resultant values of Mv and R. Note that the distance from the center is proportional to R.

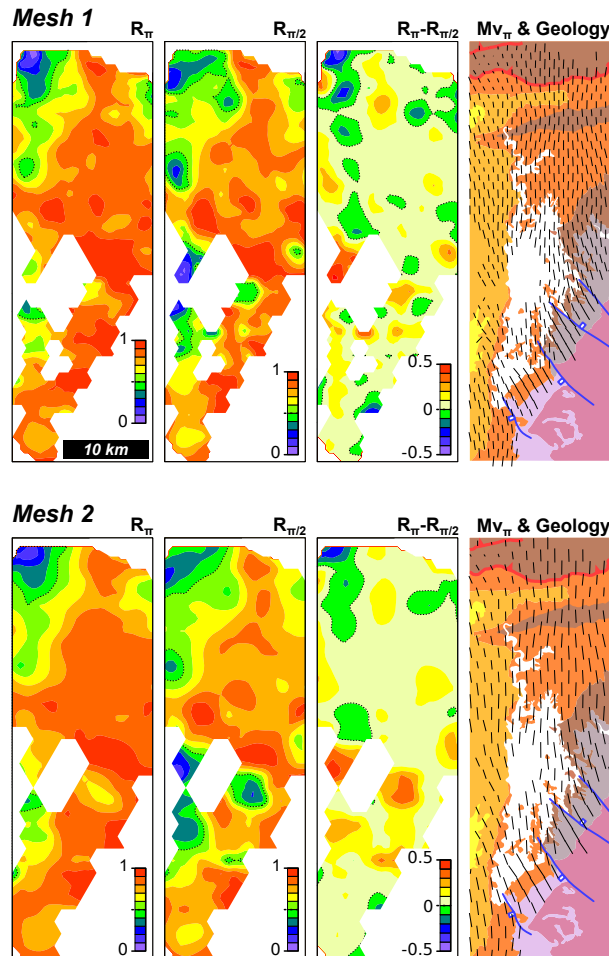


Figure 5 (Single column)

Results of circular statistics analysis for both Meshes 1 and 2. Length of traces of $Mv\pi$ is proportional to $R\pi$. Color code refers to $R\pi$ and $R\pi/2$, whereas the orientation of traces is the Mv . See text for details. .